Geomorphology 457 (2024) 109242

Contents lists available at ScienceDirect

Geomorphology

journal homepage: www.journals.elsevier.com/geomorphology

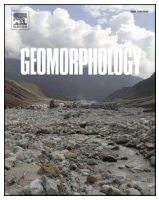

InSAR stacking to detect active landslides and investigate their relation to rainfalls in the Northern Apennines of Italy

Pierpaolo Ciuffi [a], Benedikt Bayer [b], Matteo Berti [a], Silvia Franceschini [b], Alessandro Simoni [a,*]

[a] Department of Biological, Geological and Environmental Sciences (BiGeA), University of Bologna, Via Zamboni 67, 40126 Bologna, Italy
[b] Fragile s.r.l., Via Galliera 30, 40121 Bologna, Italy

ARTICLE INFO

Keywords:
InSAR
Landslide recognition
Landslide monitoring
Rainfall threshold

ABSTRACT

Interferometric stacking is a useful technique to detect active slope deformation over vast mountainous area. Compared to the analysis of single interferograms, the stacking approach improves the signal to noise ratio and deformation signals become clearer. In this work, we used stacked interferograms to detect active slow-moving landslides during the years 2015 to 2019 over a 1200 km^2 portion of the Northern Apennines of Italy. C-band Sentinel 1 SAR images were used to create short temporal baseline (6 to 24 days) interferograms which limit decorrelation and maximize the range of measurable displacement rates. Then we operated a further selection of interferograms based on coherence and visual inspection, before stacking over multiple time scales (1 month to years). The products of the analysis are ground displacement maps where the presence of residual noise is inversely proportional to the duration of the stack and the deformation signal is clearly recognized. Results show that only a small fraction of the mapped landslide deposits are experiencing deformation that can be detected by differential interferometry. In particular, we identified 118 InSAR deformation signals corresponding to ongoing gravitational slope deformations over the 9916 landslides mapped in the area. Active movements are mostly located on landslides that have undergone catastrophic reactivation in relatively recent times. Annual interferometric stacks proved better suited to detect active slope movements, while <15 % of our deformation signals can only be detected by inspecting monthly stacks. Active slow-moving landslides show variable displacement rates in monthly stacks. Periods of dormancy alternate to accelerations that may lead to actual catastrophic failures or, more often, determine finite periods of sustained slow movement before the displacement rates drop below the detection limit. We compared the evolutionary trends of the phenomena to the occurrence of rainfall events. For this purpose, we use the probability of landslide occurrence which is associated with a rainfall event based on a territorial alert threshold. Results show that, at increasing landslide occurrence probabilities, an increasing fraction of actively deforming landslides can be detected by InSAR.

1. Introduction

Landslides are common morphological features throughout the whole Northern Apennines chain. Following the classification of Cruden and Varnes (1996), most of the landslides mapped within the study area can be described as complex landslides, which combine roto-transitional landslides with earthflows (Simoni et al., 2013). Velocities can vary from millimeters to centimeters per year during the dormant phase (which can last from years to hundreds of years) to meters per hour during the failure (e.g., Bertello et al., 2018).

Catastrophic failures typically occur after rainfall events whose duration is typically between 2 and 7 days (Berti et al., 2012). While antecedent rainfall appeared not important for landslide triggering itself (Berti et al., 2012), the relationship between displacement rate and rainfall seems to be affected by longer periods of preceding rainfall (Borgatti et al., 2006; Ronchetti et al., 2007). Moreover, surface deformation varies often for different areas of the landslide (Berti and Simoni, 2012) and the hydrological, hydrogeological conditions on a slope can be complex (Cervi et al., 2012). Anisotropy in primary conductivity, but also the presence and the formation of fissures and macropores on a landslide are difficult to assess on a slope scale, but may significantly influence infiltration, water flux, drainage and hence the build-up of pore pressure in the landslide body (Berti and Simoni, 2012). Therefore, a simple relationship between deformation and rainfall might not be

* Corresponding author.
E-mail address: alessandro.simoni@unibo.it (A. Simoni).

https://doi.org/10.1016/j.geomorph.2024.109242
Received 13 February 2023; Received in revised form 11 April 2024; Accepted 1 May 2024
Available online 6 May 2024
0169-555X/© 2024 The Authors. Published by Elsevier B.V. This is an open access article under the CC BY license (http://creativecommons.org/licenses/by/4.0/).

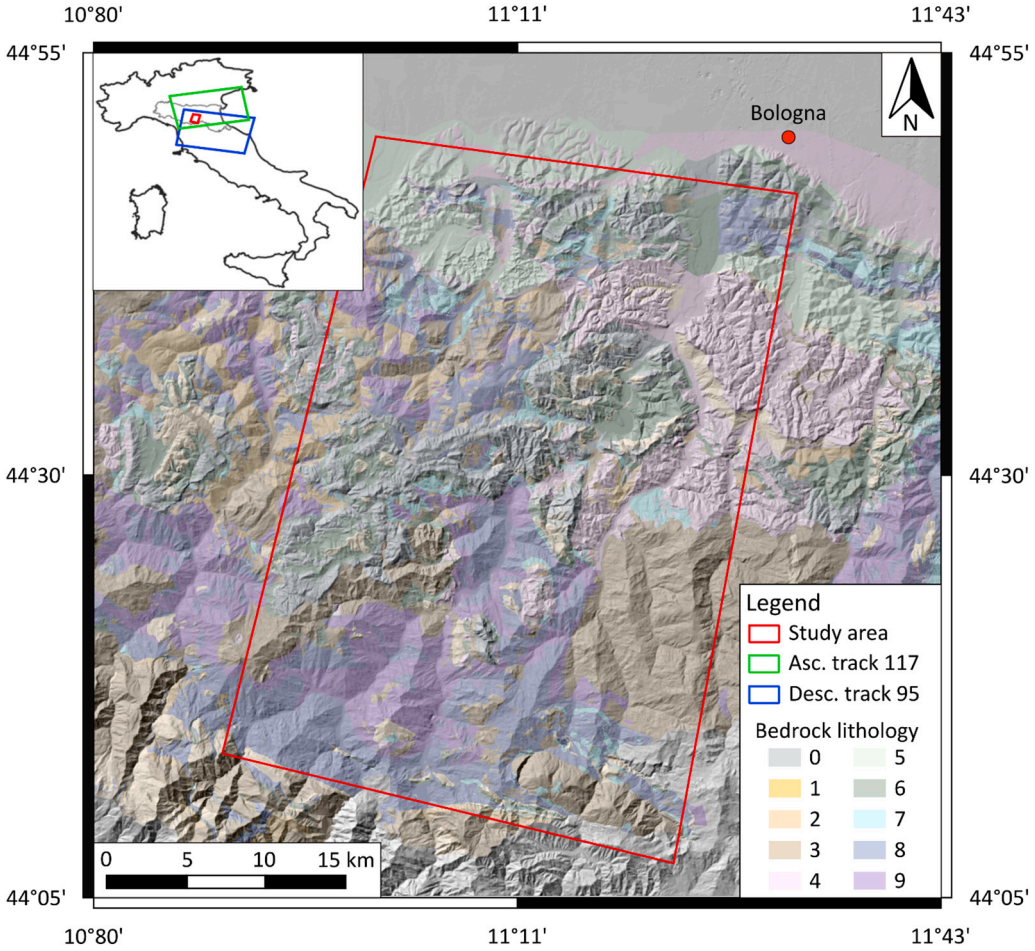

Fig. 1. Hillshade map of the study area and its location in the Italian peninsula (upper left inset). The bedrock lithologies correspond to: 0: Stone rocks, 1: Stone/Pelitic alternation with S/P > 3, 2: Stone/Pelitic alternation with 0.3 < S/P < 3, 3: Stone/Pelitic alternation with S/P < 0.3, 4: Weakly cemented sands, 5: Consolidated clays, 6: Marls, 7: Olistostromic clays, 8: Tectonized clays and argillites, 9: Palombini clays.

apparent and the detection of this relationship requires displacement and rainfall measurements with high temporal acquisition frequency.

Most slope deformation occurs in old landslide materials (Bertolini et al., 2004). In many cases, the reactivation of old deposits causes the regression of the main scarp and the physical degradation of the material which may move downwards as an earthflow. In other cases, the reactivation is more complex and different types of landslides can occur (Bertolini and Pellegrini, 2001). Monitoring landslide movements helps us better understand how the landslide mass propagates in space, how their motion evolves in time, and how external forcings, such as rainwater, control their behavior (Handwerger et al., 2019).

Conventional methods used for mapping and monitoring slope instabilities could benefit from remote sensing systems, which allow rapid and easily updatable acquisitions of data over wide areas, reducing fieldwork and costs (Ciuffi et al., 2021). A powerful technique for monitoring the displacements of large areas is the synthetic aperture radar interferometry (InSAR) that provides the possibility to measure the deformations of landslide deposits during the slow-motion stage (i.e., before the rapid acceleration). InSAR was applied in a landslide-prone area in the mid-1990s (Fruneau et al., 1996), but only in the 2000s did it became a well-known technique for landslide monitoring.

InSAR techniques can be grouped in two main families: (i) standard InSAR methods that include classic two-pass interferometry and interferometric stacking (Dini et al., 2019; Handwerger et al., 2013, 2015) and (ii) multi-temporal methods that include the so-called Persistent Scatterer Interferometry (PSI) and Small Baseline Subsets (SBAS) methods (Raspini et al., 2019; Zhang et al., 2020). In general, multi-temporal methods allow obtaining better accuracy and precision for good quality reflectors (houses, infrastructures, rock outcrops) but standard InSAR yields a more continuous coverage of a territory especially when sparse to medium vegetation cover is present. Archived and newly acquired SAR images can be interferometrically processed to extract displacement time series. These data can be used to determine the sensitivity of landslide motion to external factors such as seasonal precipitation and seismic shaking (Cohen-Waeber et al., 2018; Handwerger et al., 2015; Albano et al., 2018) and may have significant potential for detecting precursory deformation preceding catastrophic failures (Dong et al., 2018; Ciuffi et al., 2021).

This paper presents the results of a regional InSAR analysis performed by standard two-pass interferometry using C-band Sentinel 1 SAR images. The study area is represented by a 1200 km^2 portion of the Northern Apennines of Italy, and the analysis covers a period between April 2014 and December 2019. The main goal was to detect active slope movements and to investigate their evolution through time. We use interferometric stacking in order to obtain satisfactory territorial coverage also in rural areas where multi-temporal techniques typically retrieve only sparse information. Different time scales (multi-year, annual, and monthly) are considered to gauge their effect on the detection of InSAR deformation signals (IDS). We use visual interpretation together with geological judgement to detect and map InSAR deformation signals that are likely expression of gravitational slope movements. The spatial distribution of slope movements is compared to local morphology, geology of the substratum, landslide inventory and historical information. We investigate the state of activity of the

detected landslides in relation to rainfall parameters used to predict landslide occurrence on a territorial basis.

2. Study area

The study area is located in the central sector of the Northern Apennines of Italy (Fig. 1), to the west of the city of Bologna (Emilia-Romagna region). Within the study area, a total of 9916 landslide deposits have been mapped by the local Geological Survey (R.E.R., 2022). Most of these landslides periodically experience catastrophic failures (or reactivations) when displacement rates can climb up to m/day. Otherwise, they typically move at a rate of few centimeters to few tens of centimeters per year (Simoni et al., 2013).

Chaotic clay-shales with blocks in the matrix fabric (Pini, 1999; Vannucchi et al., 2003) and flysch deposits (Ricci Lucchi, 1986) are the most common lithologies in the study area (Fig. 1). Where clay shales outcrop, earthflows with distinct source, transport and deposition zones are the dominant type of slope failure (Simoni et al., 2013). Where the relief is made of pelitic flysch, a broader spectrum of landslide types can be observed, but often the failures have characteristics of translational or rotational earth- or rockslides in the upper portions of the landslide and may propagate as earthflow further down-slope (Borgatti et al., 2006; Corsini et al., 2006; Berti et al., 2017). Bertolini et al. (2004) conducted radiocarbon dating on tree logs, stumps and deposits of peat bogs that were buried inside landslide deposits of the Northern Apennines during catastrophic failures. They found ages ranging from the transition between Pleistocene and Holocene (ca. 13.759 years B.P.) and Medieval times (ca. 500 years B.P.), demonstrating the long-life cycle of these large landslides, subject to periodic reactivations and long periods of dormancy.

The Northern Apennines have a Mediterranean climate and total annual precipitation reaches on average 1300 to 1400 mm (Berti et al., 2012). The temporal pattern is characterized by intense rainfall in spring and autumn, separated by dry summers and winter months with moderate precipitation that in part occurs as snowfall (Tomozeiu et al., 2000; Pavan et al., 2008).

3. Materials and methods

3.1. InSAR analysis and detection of slope deformation signals

Space-borne synthetic aperture radar interferometry (InSAR) is a remote sensing technique which exploits the phase difference between two radar images that were acquired over a given track of the earth surface by a satellite. Part of the phase difference is caused by the deformation of the targets inside a pixel with respect to the sensor (Massonnet and Feigl, 1998; Rosen et al., 2000; Bürgmann et al., 2000). The technique has been widely used in different fields of geoscience to assess deformation processes (Hooper et al., 2004; Schmidt and Bürgmann, 2003). It provides a straightforward way to measure deformation events that occurred in the past, which is why it has been successfully applied to landsliding (Bianchini et al., 2013; Handwerger et al., 2013; Raspini et al., 2019, other citations).

InSAR, however, presents three major limitations which are related to each other.

1. Phase ambiguity: The differential phase of an interferogram is measured as a fraction of the wavelength, and a deformation field is mapped in the range between -π and π radians. At this point, the phase is generally named wrapped phase, and in deforming areas, a spatial pattern called interferometric fringes can often be observed (e.g., Rosen et al., 2000). Switching from one end of the spectrum to the other is also commonly called phase-jump. Resolving this phase-ambiguity to obtain absolute values requires a process that is called phase unwrapping and can be solved numerically by different approaches (Chen and Zebker, 2001; Hooper et al., 2007).
2. Decorrelation: Especially in rural or densely vegetated areas, decorrelation of the interferogram can happen (Zebker and Villasenor, 1992). It is mainly due to surface changes between two acquisitions (temporal decorrelation), which can result from high deformation rates, rapid vegetation growth, but also snow cover. Temporal decorrelation is more likely to occur in interferograms that span long periods. Decorrelation may also occur if the distance of the sensors between two acquisitions (known as perpendicular baseline) is large, which is called baseline decorrelation. If coherence is low, unwrapping will also be more problematic (Tarayre and Massonnet, 1996).
3. Phase noise: Even if the interferometric phase is coherent, it could contain unwanted residual noise due to the differential phase generated by DEM errors, atmospheric phase delay, and orbital inaccuracies (Tarayre and Massonnet, 1996; Zebker et al., 1997; Fattahi and Amelung, 2015; Xiao et al., 2022).

Several multi-temporal techniques, such as persistent scatterers interferometry (Hooper et al., 2004; Ferretti et al., 2001; Ferretti et al., 2011), small baseline techniques (Schmidt and Bürgmann, 2003; Berardino et al., 2002), or mixed approaches (Hooper, 2008), were developed to address the problems of decorrelation and estimate different error terms of the phase. More recently, various authors (Squarzoni et al., 2020; Handwerger et al., 2015, 2019; Ciuffi et al., 2021) have shown that traditional two-pass interferometry can be successfully used to investigate gravitational slope movements thanks to shorter satellite revisit intervals and/or improved radar image quality.

The Sentinel images used in this study are in C-band (5.6 cm radar wavelength), and they were acquired every twelve days between October 2014 and August 2016. Acquisition frequency increased to six days after the launch of Sentinel 1B Our analysis spans between April 2015 and December 2019 and considers one descending and one ascending orbit (Fig. 1).

Interferogram processing was carried out by using GMTSAR software (Sandwell et al., 2011) while the interferograms were unwrapped with SNAPHU (Chen and Zebker, 2001). We calculated and subtracted the topographic phase (e.g., Massonnet and Feigl, 1998; Bürgmann et al., 2000) by using an external digital elevation model (10 × 10 m cell size) and reduced large-scale atmospheric effects by filtering each interferogram with a high-pass filter. As stable references, we chose geomorphological features that are not affected by deformation processes, such as ridges.

Stacking interferograms improves the signal-to-noise ratio and highlights the deformation features of processes that move fast enough to observe deformation in a short period of time, but slow enough to avoid unresolvable phase jumps or decorrelation. In order to evaluate the efficiency of interferometric stacks for the mapping of active landslides for different timespans, we use three types of interferometric stacks: multi-years (covering the entire analysis period), annual and monthly. In our study area, interferograms show a rapidly deteriorating quality (i.e., higher decorrelation) with duration. Therefore, we use interferograms with a duration ranging from 6 to 30 days to form all our stacks. Interferograms showing high decorrelation are discarded before stacking. Sometimes, typically during spring or early summer, the rapid growth of vegetation causes decorrelation and does not allow obtaining a sufficient number of interferograms for stacking on a monthly basis. Based on purely theoretical considerations (Liu and Mason, 2017), maximum displacement rates measurable by using C-band SAR images and 30 days interferograms are about 340 mm/yr along the satellite LOS (Line Of Sight). In our stacks, we rarely find rates exceeding 100–150 mm/yr mostly due to averaging, unresolvable phase jumps and decorrelation.

The interpretation of interferometric stacks, obtained for the two orbits, led to the identification and mapping of InSAR deformation signals that are caused by active landslides. Other authors have used similar approaches to recognize active deformation processes on a

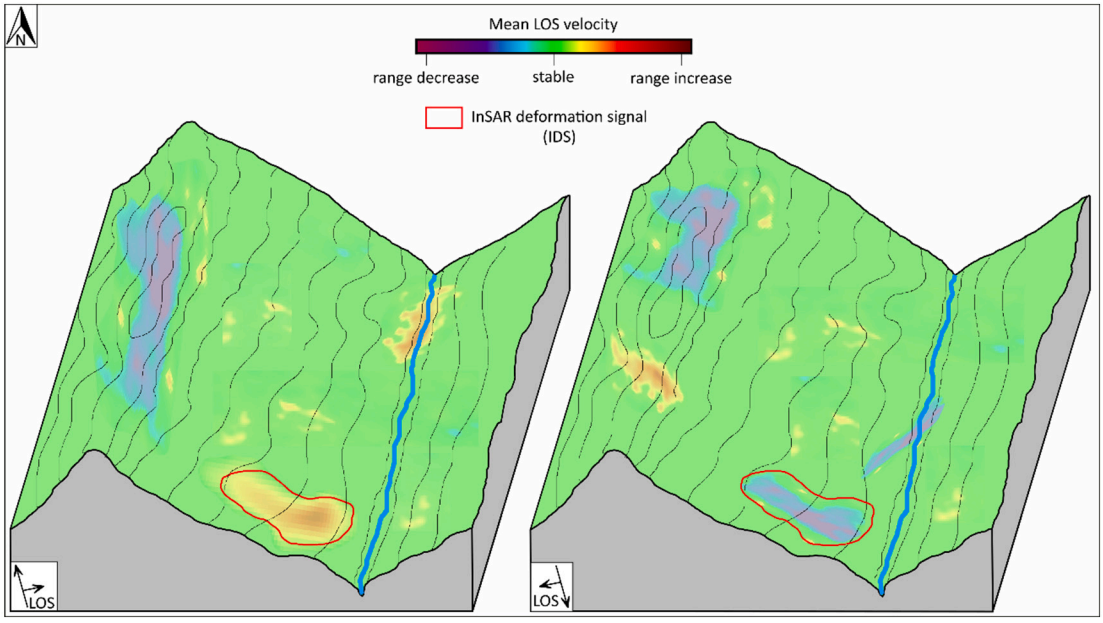

Fig. 2. Conceptual representation of a slope where an InSAR deformation signal (red polygon) is identified together with other signals likely attributable artifacts and/or noise of the interferometric data.

regional scale (Handwerger et al., 2015; Tong and Schmidt, 2016; Ciuffi et al., 2021). Our interpretation is mostly based on the local morphology described by the Digital Elevation Model (shaded relief map, slope map) and visible in aerial photographs. All IDSs are located along slopes where landslide morphology is clearly recognizable or, at least, where slope movements are consistent with the geomorphological context. An InSAR deformation signal was such when: 1) the signal does not cross a valley floor or a ridge; 2) the signal is clearly visible within the multi-year stack (in at least one orbit); 3) the signal is detectable within one (or more) annual stacks in at least one of the two orbits; 4) the signal is detectable within several monthly stacks (in at least one of the two orbits). These InSAR Deformation Signals will hereafter be referred to as IDSs.

The IDSs that we associate with active slope movements are typically patches exhibiting relatively high LOS velocities and high standard deviation of LOS velocity because ongoing deformation often produces an uneven displacement field. In addition, comparative analysis of the interferometric stacks derived from the two orbits reveals that IDSs very often show inversion of the sign of the LOS displacement. For instance, if a slope faces towards west, the deformation signal is registered as range decrease in the ascending viewing geometry, while the descending orbit measures a range increase. The inversion is compatible with displacements whose horizontal component prevails over the vertical one, such as sliding down a moderately inclined slope. Fig. 2 shows a conceptual slope in which a typical IDS is shown together with InSAR signals that cannot be interpreted as slope deformations, likely topographic artifacts (Massonnet and Feigl, 1998) or the effect of changes occurred at the surface (Liu and Mason, 2017).

We classified the slope deformation signals depending on the interferometric stacks which led to their detection. The category "multi-years, annual and monthly" includes IDSs detected in multi-years, annual and one or more monthly stacks. The category "annual and monthly" includes signals recognized as active in at least one annual and one monthly stacks which are not visible in multi-year stack. Finally, the category 'monthly' includes IDSs with deformation signals visible only in one (or more) monthly stacks but go undetected in annual and multi-year stacks. The choice of the above categories derives from the fact that all signals which recognized in multi-year stacks are visible also in one or more annual stacks. The same applies to annual signals which can

Table 1
Control elements and classes used for the analysis.

Control elements	Classes
Aspect	8 classes of 45° width
Slope gradient	5 classes of 5° width (0° to 25°) + 6th class for higher values
Quaternary deposit	1) No data 2) Slope deposits 3) Active landslides 4) Dormant landslides
Time from last known landslide Reactivation	0) No historical reactivation reported 1) Last reactivation: 1 to 30 years 2) Last reactivation: 31 to 60 years 3) Last reactivation: 61 to 90 years 4) Last reactivation: 91 to 120 years 5) Last reactivation: over 121 years 6) No data
Land use	0) Urbanized areas 1) Mining areas, quarries, landfills, artifact soils 2) Artificial green areas, parks 3) Agricultural land: arable land 4) Agricultural land: vineyards and orchards 5) Agricultural land: permanent meadows 6) Heterogeneous agricultural soils 7) Wooded areas 8) Shrub and/or herbaceous areas 9) Area with sparse or absent vegetation 10) Water environment: rivers, lakes
Bedrock lithology	0) Stone rocks 1) Stone/Pelitic alternation with $S/P > 3$ 2) Stone/Pelitic alternation with $0.3 < S/P < 3$ 3) Stone/Pelitic alternation with $S/P < 0.3$ 4) Weakly cemented sands 5) Consolidated clays 6) Marls 7) Olistostromic clays 8) Tectonized clays and argillites 9) Palombini clays

Table 2
Intersections between InSAR deformation signals and classes of control elements.

	Control element ($V_{i,j}$)	
	Present (1)	Absent (0)
IDS present (1)	N_{pix1}	N_{pix2}
IDS absent (0)	N_{pix3}	N_{pix4}

always be recognized in one or more monthly stacks.

3.2. Spatial distribution of slope deformation signals

The spatial distribution of IDSs was compared with the geological and geomorphological features of the territory in order to establish any mutual spatial relationships. In the following, such features are named control elements and include bedrock lithology, land use, slope gradient, slope exposure, quaternary deposit, and time from last known landslide reactivation. The latter is based on the information reported by the regional inventory and historical archive of landslides that is regularly updated by the authority (R.E.R., 2022).

For this analysis, we adopted a well-established technique (Meyer et al., 2014; Regmi et al., 2010) based on the theory of evidence weights (WOE) (Bonham-Carter, 1994). The WOE is a data-driven method (Bonham-Carter, 1994), which is basically the Bayesian approach in log-linear form (Spiegelhalter, 1986). The WOE uses the concept of prior (unconditional) and posterior (conditional) probability for assessing the relation between a target factor (in our case the IDSs) and several control elements spatially distributed in the area.

The control elements and the classes used for the analysis are reported in Table 1. Aspect and slope are derived from the 10 m cell-size Digital Elevation Model. The classes of bedrock lithology are obtained by grouping the geological formations (Panini et al., 2002) based on their age and expected geomechanical behavior. The Quaternary deposits include active landslides, dormant landslides, and slope deposits. Active landslides are landslides that, at the time of the survey, showed evidence of movements on a geomorphological basis. Active landslides also include landslide deposits that at the time of the survey did not show definite signs of movement, but which nevertheless denoted recent activity signaled by evident clues (impacts to artifacts, absent or scarce vegetation, remobilized soil). Dormant landslides are gravitational deposits with no evidence of current or recent movements. They generally show a regular profile, a vegetation cover with a degree of development similar to that of the surrounding areas, and absence of recent damage to artifacts such as buildings or roads. Dormant landslides can be reactivated, since the preparatory and triggering causes that led to the failure are still present. Slope deposits are defined as deposits resulting from gravitational slope processes of an uncertain nature, given poor field evidence. Genesis may be gravitational, by surface runoff or by solifluction. Information on the timing and location of catastrophic failures of landslides (R.E.R., 2022) were used to derive the 'time from last reactivation' control element. Land use information is updated to 2020 based on high-resolution (20 cm) aerial photographs and includes 10 classes (R.E.R., 2020).

The control element rasters were cross-referenced with the IDS inventory. For each class j of the control elements V_i (with $j = 1…n$), we evaluated the number of cells corresponding to the four possible combinations of the confusion matrix (Table 2). The data are used as basic information for the determination Contrast (C). C is a statistical parameter that expresses the degree of correlation between a given factor (the class of a control element, $V_{i,j}$) and the dependent variable (in our case the IDSs).

The Contrast is obtained from the difference of the weights $W^{+}_{i,j}$ e $W^{-}_{i,j}$:

$$C_{i,j} = W^{+}_{i,j} - W^{-}_{i,j} \quad (1)$$

where:

$$W^{+}_{i,j} = log\left\{\left[N_{pix1}/\left(N_{pix1}+N_{pix2}\right)\right]/\left[N_{pix3}/\left(N_{pix3}+N_{pix4}\right)\right]\right\}$$

$$W^{-}_{i,j} = log\left\{\left[N_{pix2}/\left(N_{pix1}+N_{pix2}\right)\right]/\left[N_{pix4}/\left(N_{pix3}+N_{pix4}\right)\right]\right\} \quad (2)$$

$W^{+}_{i,j}$ expresses the probability of finding a specific class ($V_{i,j}$) in an IDS. In the other hand, $W^{-}_{i,j}$ expresses the degree of anticorrelation of that class with the dependent variable. If the value of C is positive ($C > 0$), the class of the control element is favorable to the development of an IDS; if, on the other hand, the value of C is negative ($C < 0$), it is unfavorable. When C is small, there is no statistical correlation between IDSs and the considered factor-class.

Uncertainty has to be considered when interpreting C values. In general, we can say that the uncertainty increases when a certain factor-class occupies a small portion of the area. With the aim of estimating the uncertainty associated with C, we used a bootstrapping technique. This approach involves the generation of N synthetic rasters of random polygons whose size and total area are comparable to those of IDSs. Each synthetic raster is then intersected with control elements (Table 1) and the C values (N contrast values for each class of control element, $V_{i,j}$) are computed. The mean value and standard deviation of C is then calculated for each $V_{i,j}$. We adopt the standard deviation to describe the statistical variability and evaluate the uncertainty associated with C, calculated for mapped IDS. When C, considering the associated uncertainty, is greater (or less) than zero, the control element is positively (or negatively) correlated with the presence of IDS.

3.3. Velocity time series of IDS

To derive velocity information of all mapped IDSs we use monthly interferometric stacks. In general, when a landslide moves in the downslope direction and the horizontal component is larger than the vertical, the radar signal will show a range increase in one viewing geometry and, range decrease in the other. Theoretically, if the vertical

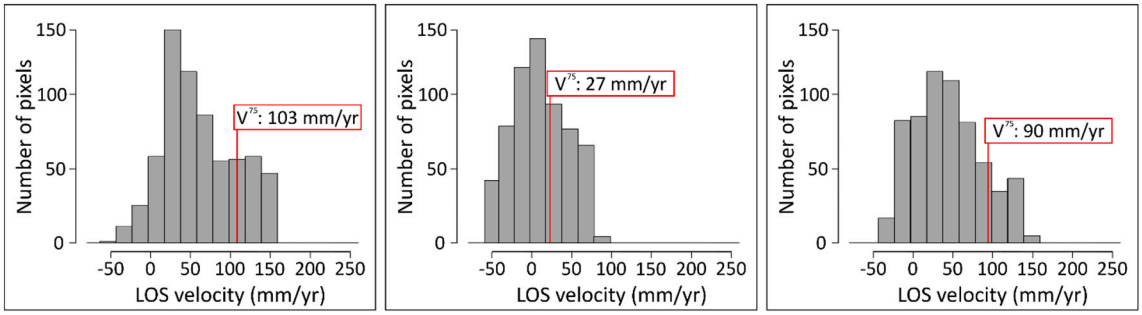

Fig. 3. Frequency histograms of LOS velocities from monthly stacks for IDS #6 (see Fig. 13). In April 2018 (left) and February 2019 (right) the distributions and their V_{75} values indicate that the landslide is actively moving. In January 2019 (middle), the landslide is dormant.

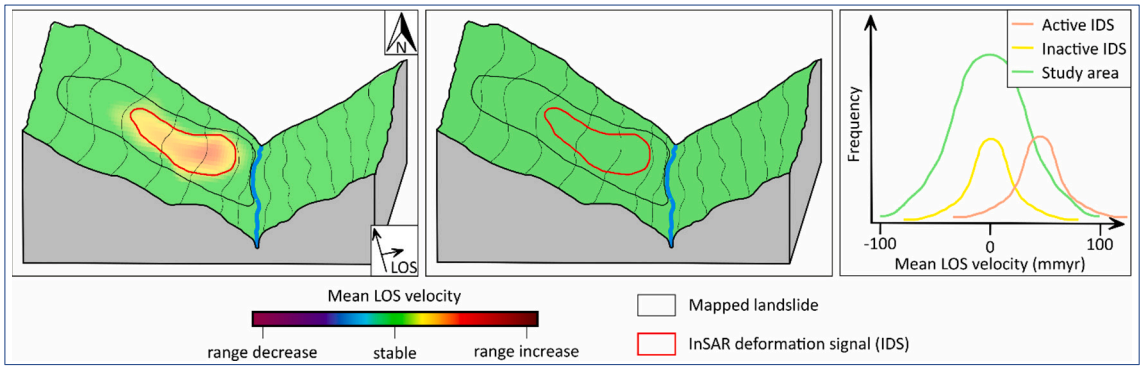

Fig. 4. Conceptual representation illustrating the binary classification of the IDS activity. The two sketches illustrate an active deformation stage (left) and a dormant stage (center). The graph on the right illustrates ideal distributions of LOS velocities derived from a monthly interferometric stack during the different stages.

component (i.e., rotational sliding) is relevant, the range may increase in both geometries, due to the lowering of the ground surface. This is rarely observed along the relatively gentle slopes of our study area. To limit complexity, we use the viewing geometry registering a range increase to extract the IDS velocities.

The LOS displacement rate of an IDS, in each monthly interferometric stack, is described by the pixel values in the IDS polygon. Their number is several hundred and their distribution typically shows a positive skewness, particularly when the signal is active (Fig. 3). We use the 75th percentile of the LOS velocity values (V_{75}) as a descriptor of the landslide velocity because we are interested in the high values of the distribution describing the most active portions of the landslide. In fact, it can happen that only portions of the mapped signal move and that the rest are still, slower or affected by residual noise. When the decorrelation compromises our ability to recognize the signal, we assign 'no value' to V_{75}.

3.4. Comparison between IDS velocities and rainfall

The comparison between InSAR-derived displacement rates and rainfall parameters necessarily requires some adjustments. We face problems that pertain to the low temporal resolution of InSAR data, to

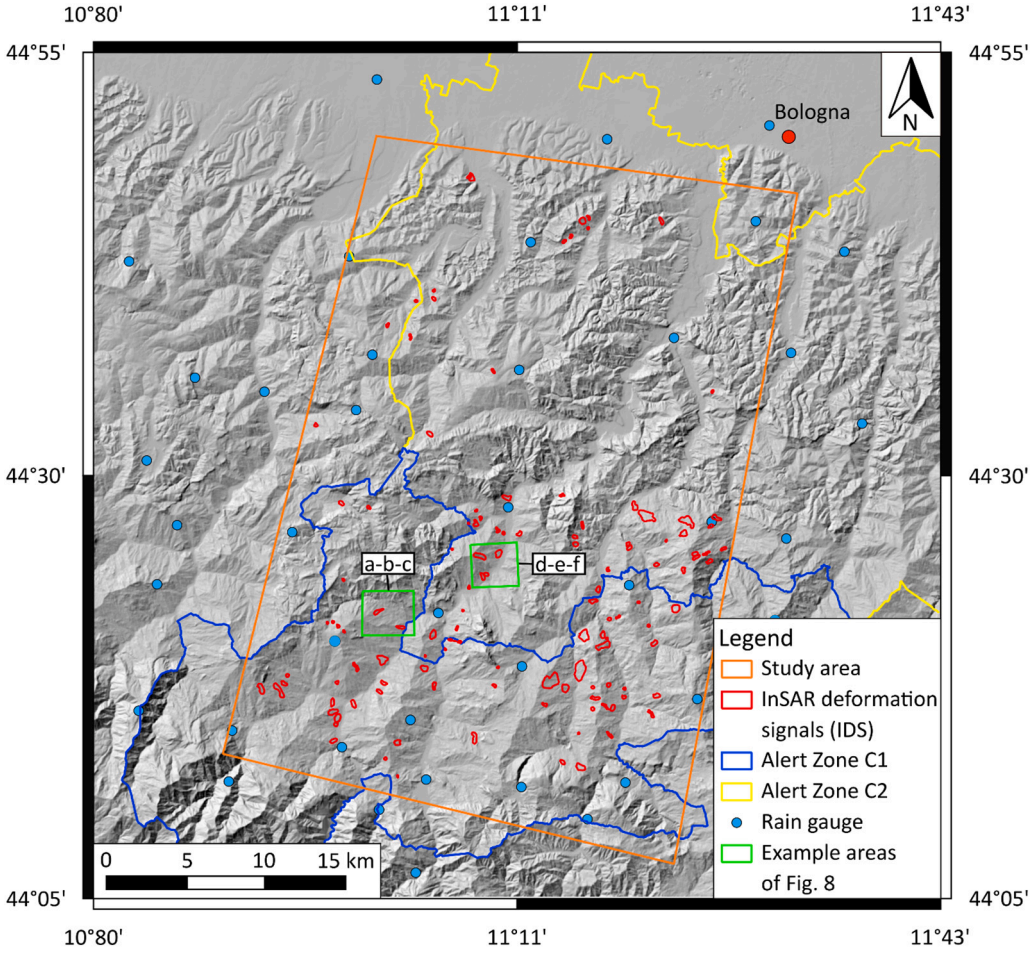

Fig. 5. Shaded relief map of the study area and spatial distribution of InSAR deformation signals (IDS). The map reports also the two Alert Zones for which aggregate rainfall values were used.

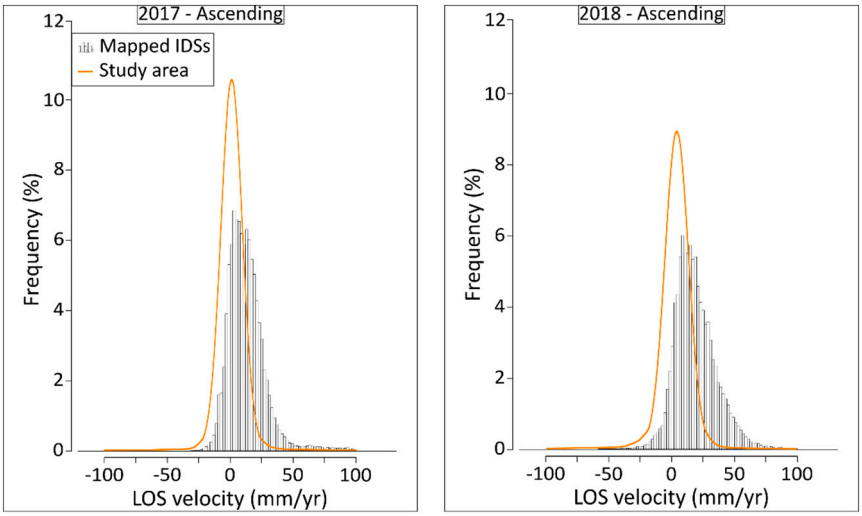

Fig. 6. Comparison of velocity distribution for the study area and the 118 mapped IDSs. Velocity values are extracted from annual stacks and are for the years 2017 and 2018.

the spatial variability of rainfalls and to the objective definition of rainfall event. Therefore, we use an approach based on the binary classification of both deformation signal velocities and rainfall.

The binary classification of landslide activity is based on a limit value of V_{75}. Such value is derived from the visual interpretation of monthly interferometric stacks: it distinguishes the 'active state' (i.e. a clearly recognizable deformation signal) from the 'inactive state' (i.e. a weak or absent deformation signal). Examples will be presented in Section 4.3.

Fig. 4 shows a conceptual slope in which an IDS was recognized and illustrates how we classify its state of activity. Based on the interpretation of interferometric monthly stacks, the V_{75} limit value is set at 55 mm/yr for all mapped IDSs. The adoption of a limit value is required for classification and represents the summary of our observations on diverse deformation signals. However, it cannot be associated with a precise meaning, especially since V_{75} is influenced by the relative orientation between LOS and ground displacement vector.

Fig. 4 on the right shows the distribution of the velocity values of stable areas outside the IDSs and IDSs during inactive states. They also show the distribution of IDS velocities during active states. This difference in the distributions shows how the IDSs have a distinct 'footprint' with respect to the study area and justifies the identification of the activity threshold.

Although there is general agreement on the importance of precipitations as landslide triggering factor (Guzzetti et al., 2020), the evaluation of the triggering rainfalls over a large territory can be very complicated, also given the possible role of antecedent rainfalls. For our analysis, we rely on the aggregated rainfall data that are used by the Emilia Romagna Region Civil Protection for their landslide early warning system. They are based on the measurements taken by tens of rain gauges within the so-called Alert Zones (Fig. 5). In our case, the Alert Zones are two: area C1 covers the upper part of the area up to the main divide, area C2 covers the lower part and extends to the plain.

Since rainfall measurements are available at much higher resolution than InSAR-derived landslide activity information, it is necessary to downsample the data to allow comparison. To this purpose we used the rainfall thresholds defined by Berti et al. (2012) to predict the occurrence of landslides in the Emilia-Romagna region. The authors took advantage of the historical landslide archive, which includes >4000 events whose date of occurrence is known, to investigate the relationship between landslides and rainfall parameters. They showed that landslide probability increased with higher rainfall duration and intensity, and proposed rainfall thresholds associated to increasing probability of landslide occurrence over a reference territorial unit (Alert Zone). Hence, thresholds are lines of equal landslide probability in the rainfall duration-intensity chart. Probability values refer to the entire Alert Zone, such as C1 and C2 (Fig. 5).

Based on these thresholds, we classified solar months depending on when the rainfall occurred. Each month, we check for the exceedance of the rainfall threshold associated to a given landslide probability. The months during which the threshold was exceeded by one or more rainfall events are classified as 'wet'. Otherwise, they are classified as 'dry'. The wet/dry month classification is done separately for the two areas for increasing probabilities of landslide occurrence. We selected this method, rather than taking into consideration monthly rainfalls or other precipitation parameters, because in our study area landsliding is typically triggered by intense rain events lasting a few days (Berti et al., 2012; Squarzoni et al., 2020).

4. Results

4.1. Regional and multiple temporal scales InSAR analysis

We identified and mapped active landslides by stacking interferograms on different time scales. As explained in Section 3.1, regardless of the stack duration, we use only 6 to 30 days interferograms to minimize decorrelation. Therefore, we do not expect to measure displacement rates in different ranges, depending on the stack duration. Rather, we expect to characterize the style of activity of our landslides by distinguishing, for example, slope movements which proceed slowly and with little variation through several seasons from acceleration episodes that may involve landslide deposits following rain events.

In total, through our InSAR analysis, we detected 118 active slope movements in the predominantly hilly and mountainous terrain of the study area (Fig. 5). The deformation signals have a plan area ranging from about 0.006 to 0.661 km^2, with an average of 0.81 km^2.

Fig. 6 shows the LOS velocity distribution for the study area and the 118 mapped IDSs. The velocity values shown are extracted from annual stacks, which represent the data on which most of the recognition and mapping process was carried out. The IDS distributions show notably higher velocities when compared to those pertaining to the whole study area, which appear normal and centered on null values. Also, deformation signals typically show positive skewness which translates into high peak velocities which facilitate recognition compared to the surrounding stable slopes.

Many IDSs (67) are recognized in landslide deposits mapped by the landslide inventory (Trigila et al., 2010). They show that part of the

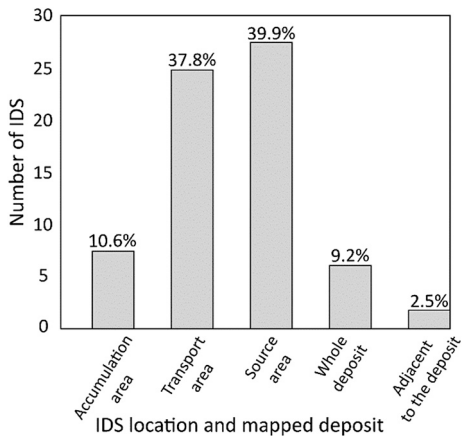

Fig. 7. Location of slope deformation signals in relation to the landslides mapped by the inventory (R.E.R., 2022).

mapped landslide deposit or the whole of it are experiencing measurable surface displacement. We classified the relative position of the IDS and the landslide. Fig. 7 shows the frequencies of the five categories that we used.

The majority of IDSs indicate that only a portion of the landslide (about 90 %) is actively deforming. Only in ten cases, we observe surface displacements across the whole mapped deposit. Active movements tend to localize in the medium and upper part of the landslide while, further downslope, the accumulation area is more often dormant. Such result is consistent with the observation that the source area is typically the most active part of the landslide and that most landslide reactivations begin with failures involving the upper/lateral scarp of the landslide and propagate downslope (Bertolini et al., 2004; Simoni et al., 2013).

Fig. 8 shows two sample portions of the study area, whose location is reported in Fig. 5, where deformation signals are mapped and appear differently depending on the stack duration: multi-year (a, d), annual

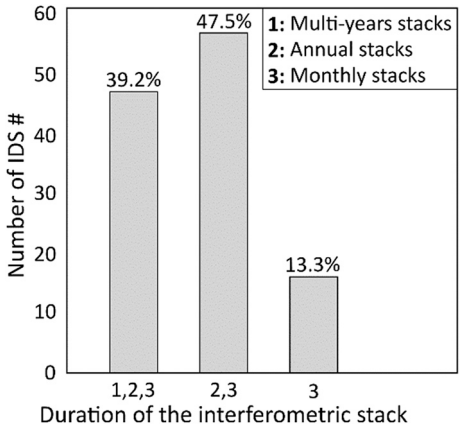

Fig. 9. Frequency of detected IDSs in stacked interferograms of different duration.

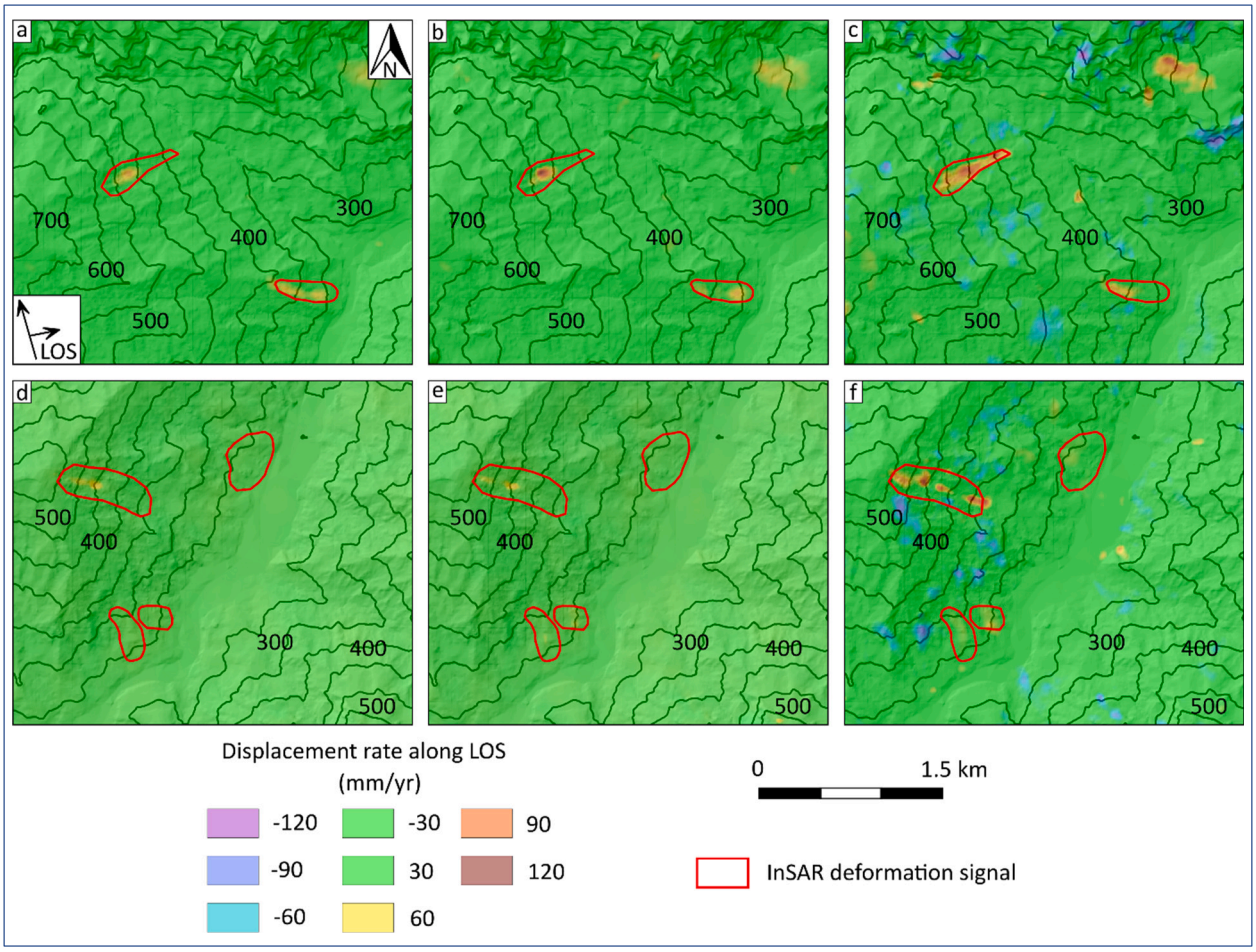

Fig. 8. Stacked interferograms of two sample areas and different duration: entire analysis period (a, d), the year 2018 (b–e) and December 2019 (c–f). The location and extent of the sample areas are reported in Fig. 6.

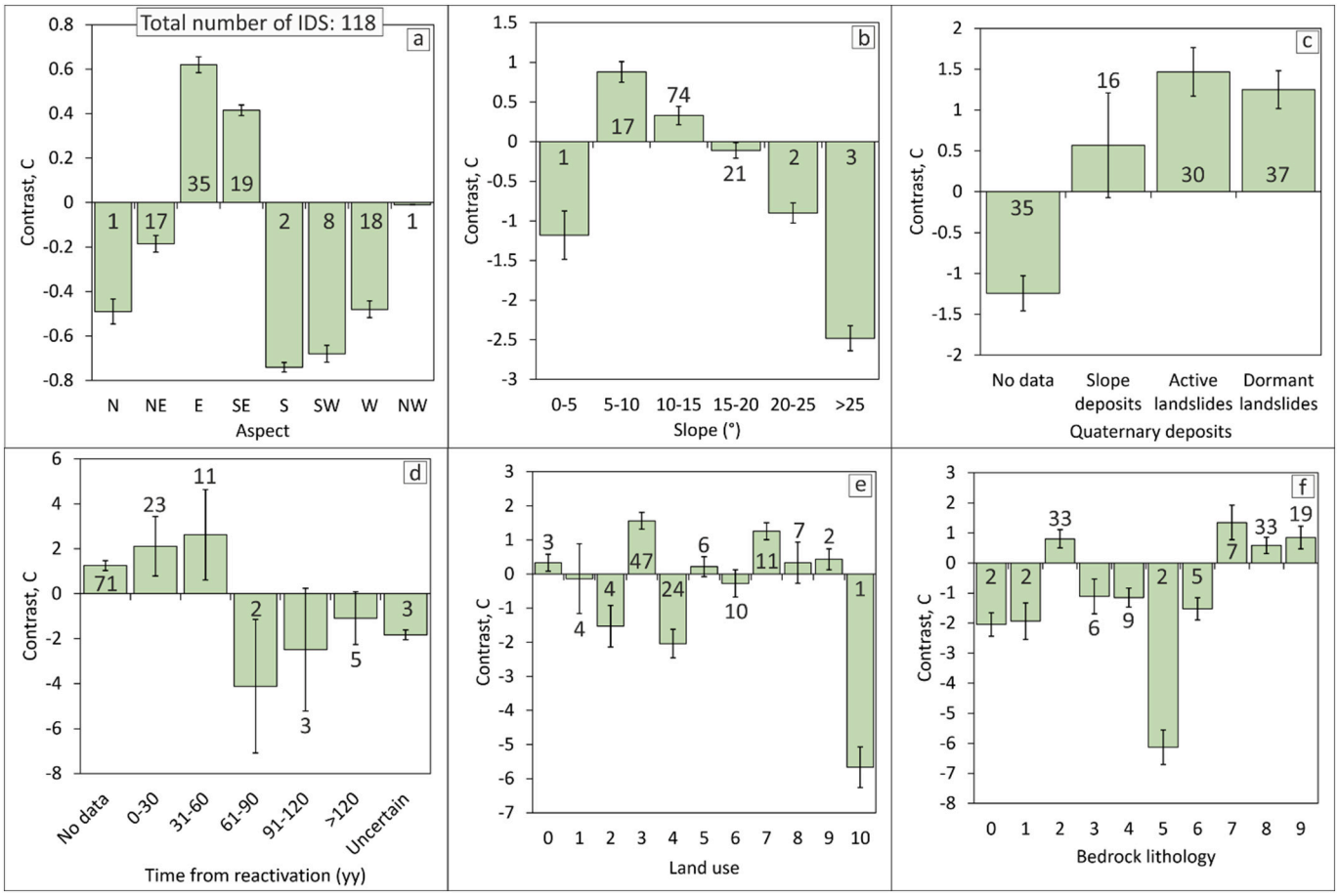

Fig. 10. Contrast index (C) values obtained for the control elements (Table 1). Positive values indicate the existence of a spatial correlation between the specific class of the control element and IDSs. Error bars describe the uncertainty associated to the correlation measure, numbers in the histograms indicate the number of IDS belonging to each class. Refer to Table 1 for key of Land use and Bedrock lithology classes.

(2018) (b, e) and monthly (December 2019) (c, f).

All interferometric stacks show a continuous coverage of the territory with residual noise (i.e., the random blue and red "spots") that is more abundant in monthly stacks and is almost absent in the annual and multi-year stacks. Signals interpreted as the effect of residual noise are preferentially located along steep, vegetated slopes and were observed throughout the entire study area.

Fig. 9 illustrates the result showing that about 40 % of the IDSs can be detected in interferometric stacks of all durations. Nearly 50 % of the IDSs are clearly detectable only in the annual and monthly stacks, while only 10 % of the signals are visible only in the monthly stacks. This result clearly indicates that the vast majority of slope deformation signals (i.e., 90 %) are clearly detectable in the annual stacks while a smaller fraction (i.e., 10 %) requires the analysis of monthly stacks for detection. Of course, visually inspecting and interpreting monthly stacks is much more time-consuming than annual stacks. Furthermore, monthly stacks contain some decorrelation due to residual noise that may complicate the interpretation and often disappears in annual stacks. On the other end of the spectrum, multi-year stacks do not offer any advantage over annual. On the contrary, about 40 % of detected signals are not appreciable in multi-year stacks, due to the progressive decline in displacement rates calculated over such a long time interval, which may include some dormancy period. Annual stacks proved the most suitable for the detection of slope movements and offer the best signal-to-noise ratio, although some occasional and short duration phenomena can be detected only in monthly stacks. These results cannot be generalized because of the diverse types of landslides, rates of movement and style of activity that can be found in other geological contexts (Cruden and Varnes, 1996).

4.2. Spatial distribution of InSAR deformation signals

By comparing the distribution of IDSs over the territory with six control elements (Table 1), we obtain an objective measure of their mutual spatial correlation. The values of the Contrast index, which is a measure of such correlation, are shown in Fig. 10 together with associated uncertainties (see Section 3.2). Results are consistent with the geological and geomorphological characteristics and strongly indicate that the distribution of IDS within the study area is not random.

Slope aspect (Fig. 10a) has a positive correlation for predominantly East and Southeast-facing slopes, while it is negative for slopes facing North, South and Southwest. For the remaining orientations, the value of the index is too low to give any meaningful indication. Overall, the correlation with the slope aspect appears to be conditioned by the orientation of the satellite's line of sight (LOS), which is oriented E-NE in the ascending orbit and W-NW in the descending orbit. In fact, North and South-facing slopes, whose movements are hardly visible in both orbits because they are approximately orthogonal to the LOS, show strong negative correlation. Due to the inherent biases deriving from LOS orientation, the analysis cannot lead to fully meaningful results regarding the aspect of active landslides. However, when interpreting the results, it must be considered that slopes have preferential orientation towards E and W in the study area (Fig. 5).

Spatial correlation with slope gradients (Fig. 10b) indicates that signals are most abundant along moderately steep slopes (7.5° to 17.5°), while the negative correlation becomes progressively stronger for higher

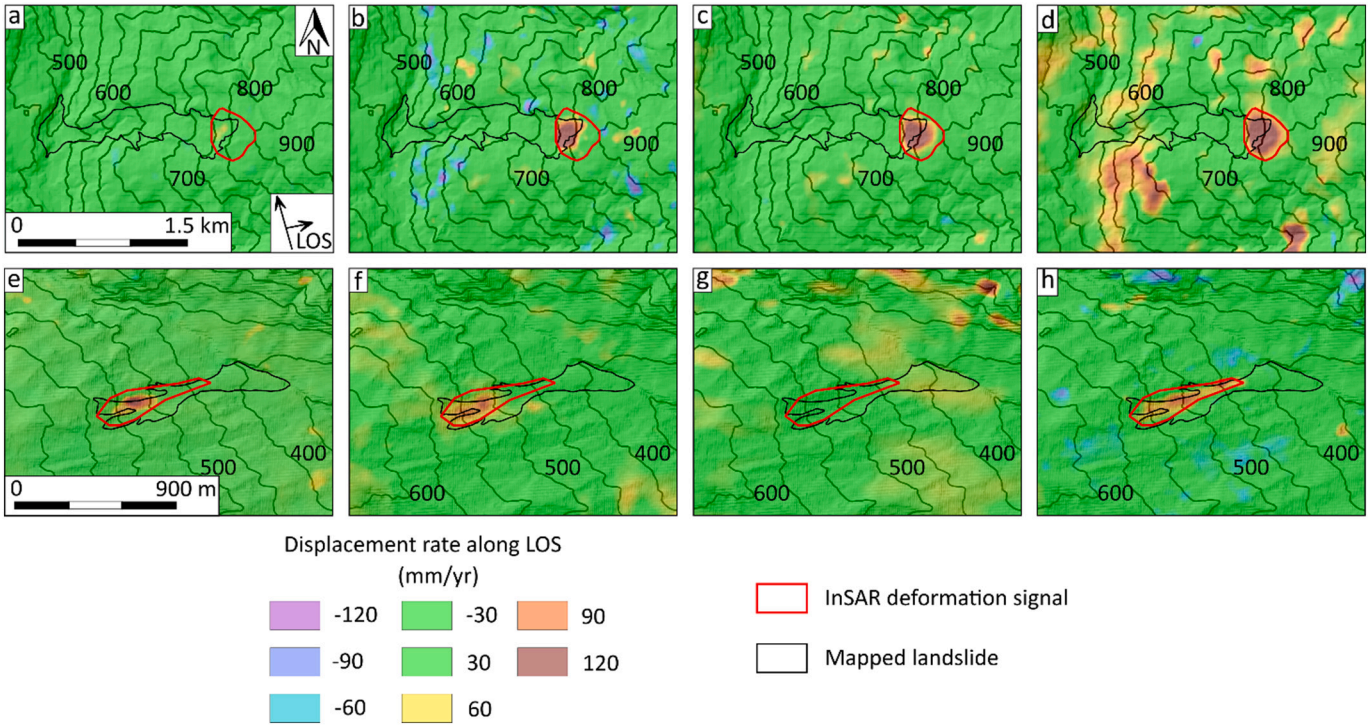

Fig. 11. Examples of monthly interferometric stacks for two example deformation signals. The sequence a–d shows the March to June 2017 period and sequence e-h shows April to July 2017 (red and black rectangles in Fig. 13, respectively).

gradients. The result is a logical consequence of weak fine-grained rocks producing gentle relief and being the most susceptible to landslides, in the Emilia Romagna region (Bertolini et al., 2002). They include pelitic flysch, clay shales and argillites. Our analysis demonstrates that the bedrock lithology has a strong influence also on the distribution of active slope movements identified by IDSs. In fact, all the landslide-susceptible lithologies (classes 2, 7, 8 and 9) are associated with significant positive values of the Contrast index while all the remaining lithologies have negative correlation with active slope deformations (Fig. 10d).

Comparing IDS with quaternary deposits, we found that mapped landslide deposits, both active and quiescent, show a significant positive correlation (Fig. 10c). On the contrary, the correlation of generic slope deposits (i.e., genesis uncertain/not recognizable) is not significant. The 35 IDS located along slopes where no deposit is mapped indicate either pre-failure deformation of incipient landslides or undetected active landslides.

The time interval since the last episode of recorded landslide reactivation can be determined thanks to the landslide archive of the Emilia-Romagna region (R.E.R., 2022). Such information is crucial to make any reasoning about event frequency and to understand the cyclic behavior of landslides. The degree of spatial correlation of IDSs and recent landslides (Fig. 10e), shows significant positive C values, up to 60 years. It should be noted, however, that the completeness of the archive decreases for older episodes and that there is no information regarding 2/3 of our signals.

Finally, comparing IDS with land use (Fig. 10f), significant positive correlations ($C \gg 0$) is found for classes 3 and 7, defined by arable land and wooded areas, respectively. The result is important in that indicates that our standard InSAR analysis is capable of territorial coverage good enough to investigate vegetated areas, at least in our study area, where slopes are gentle. Significant negative correlations are found for classes 2 (artificial green areas and parks), class 4 (vineyards and orchards) and class 10 (water environment). For the remaining classes, the correlation is non-significant.

4.3. Comparison of IDS state of activity and rainfall forcing

The intensity of the interferometric signal describes the state of activity of the slope movement and shows either no deformations (Fig. 11a, g) or ground displacement with variable degrees of activity (Figs. 11b, c, d, e, f, h).

The results of the comparison between our InSAR results and rainfall forcing can be visually inspected in Figs. 12 and 13. The graphs illustrate the behavior of IDS through time, for the two areas C1 (Fig. 12) and C2 (Fig. 13), in comparison with the distribution of wet/dry months which, in this case, are classified based on the rainfall threshold associated with a landslide probability of 60 % (see Section 3.4). The two figures show how many IDSs are in active state during a given month and allow to appreciate the evolution of all 118 slope deformation signals through time as revealed by monthly stacked interferograms. Although appreciable, the relationship between the exceedance of the rainfall threshold (blue bands) and the deformation signal reactivation/acceleration is far from mechanistic. For example, May 2017 is classified as a dry month, but many active IDS (65/118) are identified in both C1 and C2 areas. The opposite is found in November of the same year when few active IDS (6/118) are observed despite the wet month classification. Different factors may explain these findings. First, one should consider that landslide rainfall thresholds describe the probability of having at least one landslide over a large mountain territory (about 2600 km^2 on average) where thousands of landslide deposits are recognized along the slopes. The presence of many inactive landslides during a rainy month can therefore be seen as perfectly normal. Second, our monthly temporal resolution could cause the loss of some rainfall-acceleration matches (i.e., a rainfall event occurring late in the month may lead to an acceleration that is revealed only in next-month interferograms). Once a landslide has accelerated due to abundant rainfalls, its motion can persist for some time before it returns to inactive (Leroueil et al., 1996) and this may explain many active signals in dry months. Third, our InSAR analysis may miss failure episodes associated to displacement rates too high to be measured (i.e., $>100 \div 150$ mm/yr) or occurring during spring months when the rapid growth of the vegetation typically

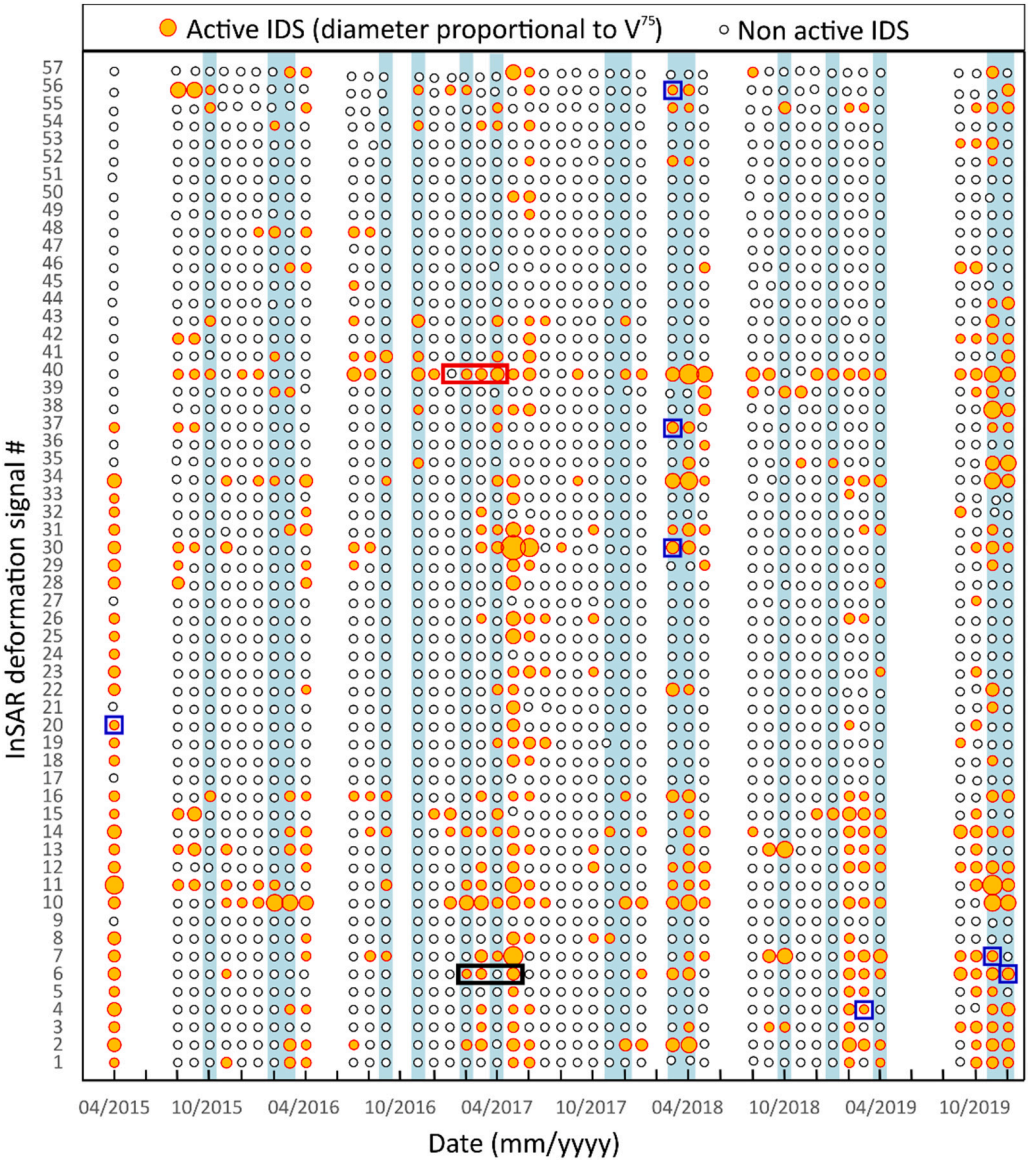

Fig. 12. Summary chart representing the state of activity and displacement rates (V_{75}) of all slope deformation signals (IDS) detected over area C1. Blue bands identify 'wet' month during which the rainfall threshold for landslide occurrence (60 %) was exceeded. Red and black rectangles identify the stacked interferograms of Fig. 11, blue squares identify landslide catastrophic reactivations documented in the regional landslide archive (R.E.R., 2022).

causes decorrelation (Squarzoni et al., 2020).

In order to explore the correlation of our slope deformation signals with rainfall, we analyze the scenarios generated by using a range of landslide probabilities. In general, higher landslide probabilities are associated to higher rainfall thresholds in the duration-intensity space which operate the selection of more 'extreme' rainfall events. The binary classification tools are used to objectively measure the results of the comparison (Fig. 14a). Each wet month, active deformation signals are counted as 'true positive' cases (tp) and inactive signals as 'false positive' (fp). Each dry month, active deformation signals are counted as 'false negative' (fn) and inactive ones as 'true negative' cases (tn). Here, we are not evaluating the goodness of the forecasting model (i.e., rainfall threshold) but rather trying to verify whether more deformation signals activate or accelerate following intense and prolonged rainfall events. Therefore, we use two common binary statistics indexes which measure the rate of IDSs showing an activity status compatible with the climatic conditions of the corresponding month. The positive predictive value, or precision (ppv) measures the rate of active deformation signals during wet months. The accuracy (acc) measures the overall rate of 'true positive' and 'true negative' cases.

$$\mathrm{ppv} = (\mathrm{tp})/(\mathrm{tp}+\mathrm{fp}) \tag{3}$$

$$\mathrm{acc} = (\mathrm{tp}+\mathrm{tn})/(\mathrm{tp}+\mathrm{tn}+\mathrm{fp}+\mathrm{fn}) \tag{4}$$

Indexes are calculated for Alert Zone landslide probabilities in the range 10 to 90 % and results are reported in Fig. 14b. It shows that both ppv and acc increase with the severity of climatic conditions (i.e., higher landslide probability). In other words, the precision index (ppv) describes the percentage of active IDSs during wet months classified based on a given rainfall threshold. By using all the rainfall thresholds associated to the range of landslide probabilities, we describe the variation of incidence of actively deforming slope movements. Similar results are obtained for the accuracy index (acc).

5. Conclusive remarks

We used standard 2-pass interferometry to investigate slope deformations in a 1200 km^2 portion of the Northern Apennines of Italy

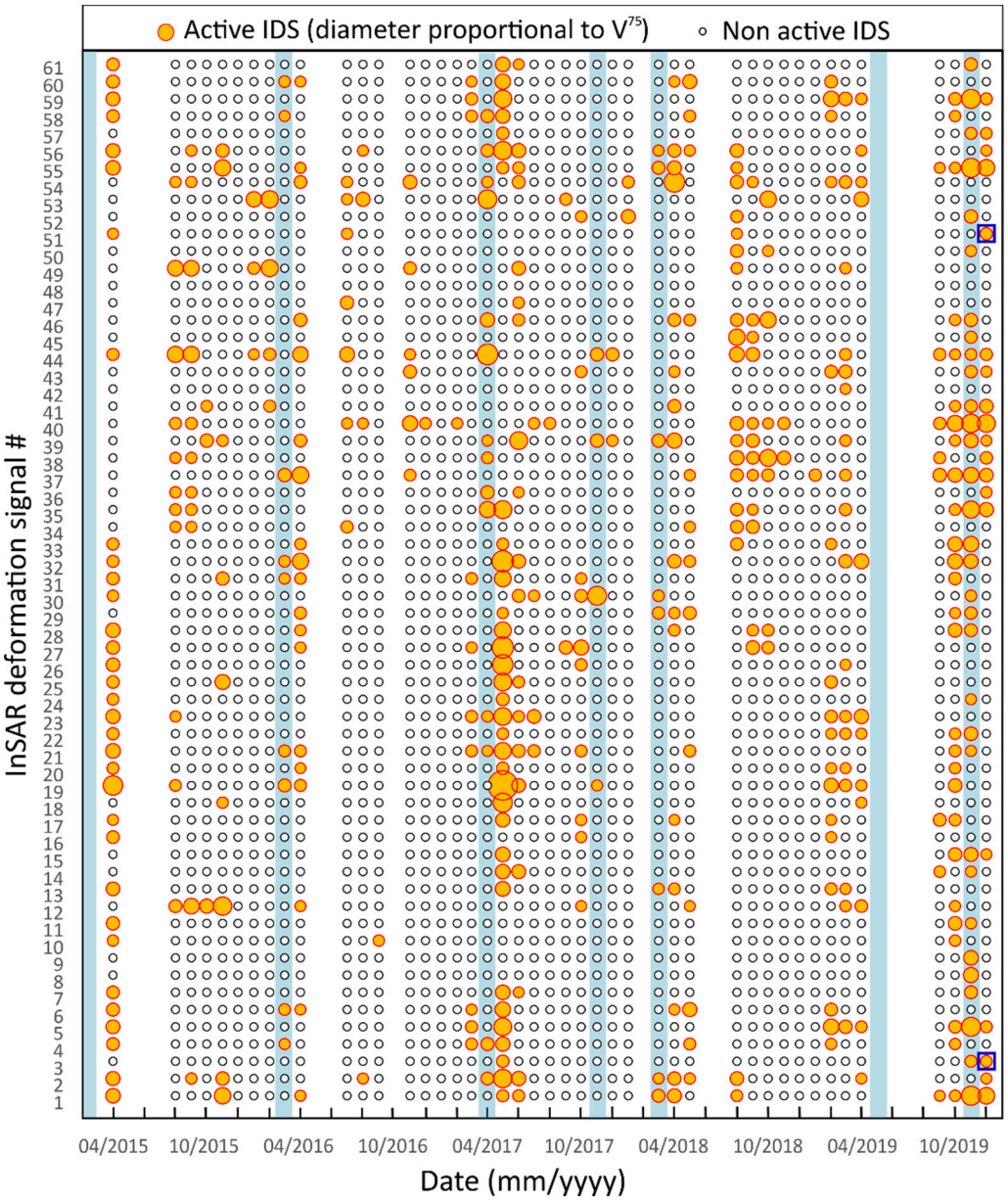

Fig. 13. Summary chart representing the state of activity and displacement rates (V_{75}) of all slope deformation signals (IDS) detected over area C2. Blue bands identify 'wet' month during which the rainfall threshold for landslide occurrence (60 %) was exceeded. Blue squares identify landslide catastrophic reactivations documented in the regional landslide archive (R.E.R., 2022).

where landsliding is widespread. Our investigation runs from April 2015 to December 2019 and makes use of short duration (6–30 days) C-band interferograms to detect active slope movements and monitor their evolution.

Results show that stacking interferograms allowed us to increase the signal-to-noise ratio and derive quasi-continuous deformation maps (Handwerger et al., 2015; Dini et al., 2019; Ciuffi et al., 2021). In our study area, these results are favored by the gentle morphology where steep slopes (>30°) are relatively rare.

Based on visual inspection and interpretation of stacked interferograms, we detected 118 active slope deformation signals (IDS) that are most likely landslides. The majority of them are better recognized in annual interferometric stacks which show very little residual noise and allow clear detection of slow sustained movements. Thirteen percent of our IDS can be detected only in monthly stacks, most likely because their activity is discontinuous in time. Multi-year interferometric stacks do not allow to identify further phenomena compared to annual stacks, instead nearly half of the IDSs detected in these latter are no longer recognizable due to averaging over multiple years. When compared to the number of landslides mapped by the regional inventory, our active slope deformation signals account for only 1.2 %, indicating that a large number of landslide deposits did not experience detectable displacement rates (>30 mm/year approx.) during the study period.

Our inventory of active slope movements may be incomplete because of some deformations could go undetected due to their small extension (<0.2 km^2 approx.), fast pace (>100 ÷ 150 mm/yr) or location along steep, unfavorably oriented slopes. On the other hand, deformation signals detected by our analysis of stacked interferograms, show remarkable correlation with the geological and geomorphological parameters typically associated to landsliding in our study area. Most of the IDSs are located along slopes consisting of weak, fine-grained lithologies with slope gradients between 5 and 15°, reflecting the landslide susceptibility of the study area (Simoni et al., 2013). Positive spatial correlation is found with landslide deposits mapped in the

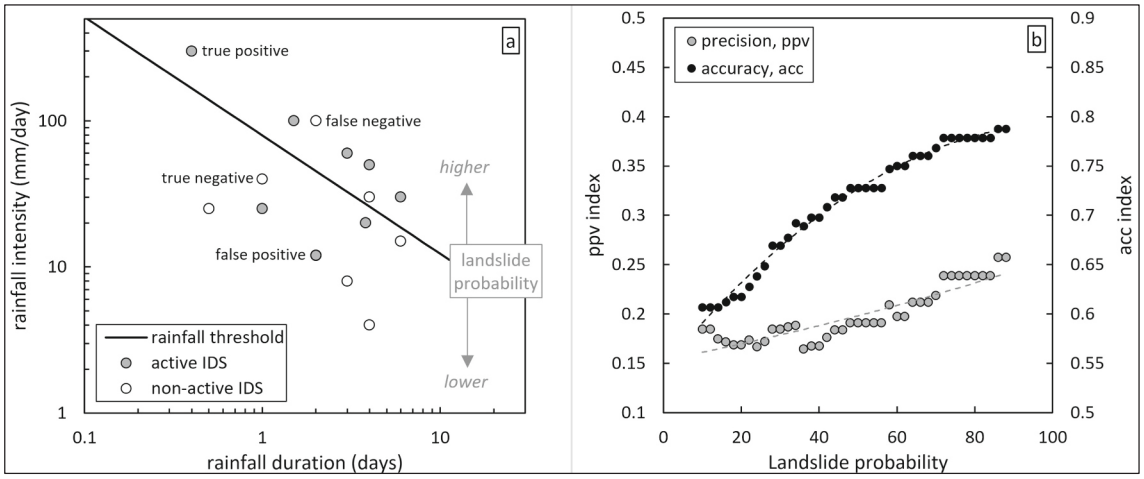

Fig. 14. a) Conceptual representation of the binary classification used to compare the state of activity of IDSs to the rainfall conditions described by the exceeding, or not, of the rainfall threshold. b) Rate of active deformation signals during 'wet' months (ppv) and overall rate of IDS activity coherent with rainfall conditions (acc) for increasing landslide probabilities predicted by rainfall thresholds for the Alert Zone.

regional inventory and, among them, phenomena that experienced catastrophic failures in the last decades have higher chances of being subject to active deformation.

The use of interferometric stacks for the detection and mapping of active deformation signals shows its usefulness as a tool for landslide hazard recognition. It allows to identify the active portions of landslides even in areas where stable reflectors are scarce or absent. By using short duration interferograms, it pushes the upper limit of the measurable displacement rates to over 100 mm/yr, which exceeds the rates measurable by multi-temporal InSAR techniques (Raspini et al., 2019). Although our displacement measurements are not as accurate as those obtained by multi-temporal InSAR (Cohen-Waeber et al., 2018), or by ground-based monitoring, interferogram stacking appears a viable method to detect active slope movements in rural mountain areas where good quality scatterers are scarce or absent.

We pushed our analysis further by analyzing a large number of stacked interferograms pertaining to short monthly intervals and found satisfactory results in capturing the variable degree of activity (i.e., displacement rate) exhibited by our slope deformation signals over time. Not all monthly stacks can be used for this purpose: about 30 % of the total are discarded due to decorrelation which is more common in the spring months when the vegetation grows rapidly (Squarzoni et al., 2020) or in the winter months when some snow cover is present (Manconi, 2021). The resulting displacement rate time series were compared to rainfall forcing making use of the rainfall thresholds associated with territorial landslide probabilities (Berti et al., 2012). In general, we observe a good correspondence between rainfall and IDS activation. Considering increasing landslide probabilities (i.e., heavier rainfalls), the percentage of actively moving landslides increases. During dry months, a relevant fraction (about 15 %) of our slow-moving landslides still exhibit appreciable deformation indicating that its motion can persist for some time.

Our work contributes to expand the possible applications of standard InSAR in the broad field of landslide risk management. Standard InSAR acquired significance in such context is thanks to the decrease of the revisit times of the satellites (Torres et al., 2012), which determines a substantial decrease of decorrelation. Longer wavelength sensors (Filippazzo and Dinand, 2017) might further contribute in the near future to increase the performance of satellite radar interferometry in rural areas. Interferogram stacking appears as an efficient tool to update existing landslide inventories and/or create inventories of active slope movements. Our analysis indicates that it can also be used as an instrument of territorial surveillance and monitoring over large mountain areas.

CRediT authorship contribution statement

Pierpaolo Ciuffi: Writing – original draft, Methodology, Investigation. **Benedikt Bayer:** Supervision, Methodology, Investigation, Data curation, Conceptualization. **Matteo Berti:** Methodology, Investigation. **Silvia Franceschini:** Methodology, Investigation. **Alessandro Simoni:** Writing – review & editing, Writing – original draft, Methodology, Investigation, Conceptualization.

Declaration of competing interest

The authors declare that they have no known competing financial interests or personal relationships that could have appeared to influence the work reported in this paper.

Data availability

Data will be made available on request.

Acknowledgements

The authors would like to thank Jeff Coe for his thorough revision of the text and constructive comments that helped improve the manuscript in its current form. We acknowledge financial support under the National Recovery and Resilience Plan (NRRP), Mission 4, Component 2, Investment 1.1, Call for tender No. 104 published on 2.2.2022 by the Italian Ministry of University and Research (MUR), funded by the European Union – NextGenerationEU– Project Title MIRAGE: Mass movement Investigation and prediction through geomorphology, Remote sensing and Artificial intelliGEnce – CUP J53D23002880006-Grant Assignment Decree No. 965 adopted on 30/06/2023 by the Italian Ministry of Ministry of University and Research (MUR).

Appendix A. Supplementary data

Supplementary data to this article can be found online at https://doi.org/10.1016/j.geomorph.2024.109242.

References

Albano, M., Saroli, M., Montuori, A., Bignami, C., Tolomei, C., Polcari, M., Pezzo, G., Moro, M., Atzori, S., Stramondo, S., Salvi, S., 2018. The relationship between InSAR Coseismic Deformation and Earthquake-induced landslides associated with the 2017 Mw 3.9 Ischia (Italy) earthquake. Geosciences 8, 303. https://doi.org/10.3390/geosciences8080303.

Berardino, P., Fornaro, G., Lanari, R., Sansosti, E., 2002. A new algorithm for surface deformation monitoring based on small baseline differential sar interferograms. IEEE Trans. Geosci. Remote Sens. 40, 2375–2383.
Bertello, L., Berti, M., Castellaro, S., Squarzoni, G., 2018. Dynamics of an active earthflow inferred from surface wave monitoring. J. Geophys. Res. Earth 123, 1811–1834. https://doi.org/10.1029/2017JF004233.
Berti, M., Simoni, A., 2012. Observation and analysis of near-surface pore-pressure measurements in clay-shales slopes. Hydrol. Process. 26, 2187–2205. https://doi.org/10.1002/hyp.7981.
Berti, M., Martina, M.L.V., Franceschini, S., Pignone, S., Simoni, A., Pizziolo, M., 2012. Probabilistic rainfall thresholds for landslide occurrence using a Bayesian approach. Case Rep. Med. 117, F04006.
Berti, M., Bertello, L., Bernardi, A.R., Caputo, G., 2017. Back analysis of a large landslide in a flysch rock mass. Landslides. https://doi.org/10.1007/s10346-017-0852-5.
Bertolini, G., Pellegrini, M., 2001. The landslides of the Emilia Apennines (northern Italy) with reference to those which resumed activity in the 1994–1999 period and required civil protection interventions. Quad. Geol. Appl. 8, 27–74.
Bertolini, G., Canuti, P., Casagli, N., De Nardo, M., Egidi, M., Mainetti, M., Pingone, R., Pizziolo, M., 2002. Carta della Pericolosità Relativa da Frana della Regione Emilia-Romagna. SystemCart, Rome, Italy.
Bertolini, G., Casagli, N., Ermini, L., Malaguti, C., 2004. Radiocarbon data on late glacial and holocene landslides in the Northern Apennines. Nat. Hazards 31, 645–662.
Bianchini, S., Herrera, G., Mateos, R.M., Notti, D., Garcia, I., Mora, O., Moretti, S., 2013. Landslide activity maps generation by means of persistent scatterer interferometry. Remote Sens. 5, 6198–6222. https://doi.org/10.3390/rs5126198.
Bonham-Carter, G.F., 1994. Geographic Information Systems for Geoscientists: Modeling With GIS. Pergamon Press, Canada.
Borgatti, L., Corsini, A., Barbieri, M., Sartini, G., Truffelli, G., Caputo, G., Puglisi, C., 2006. Large reactivated landslides in weak rock masses; a case study from the Northern Apennines (Italy). Landslides 3 (2), 115–124.
Bürgmann, R., Rosen, P.A., Fielding, E.J., 2000. Synthetic aperture radar interferometry to measure Earth's surface topography and its deformation. Annu. Rev. Earth Planet. Sci. 28, 169–209.
Cervi, F., Ronchetti, F., Martinelli, G., Bogaard, T.A., Corsini, A., 2012. Origin and assessment of deep groundwater inflow in the Ca′ Lita landslide using hydrochemistry and in situ monitoring. Hydrol. Earth Syst. Sci. 16 (11), 4205–4221.
Chen, C.W., Zebker, H.A., 2001. Two-dimensional phase unwrapping with use of statistical models for cost functions in nonlinear optimization. JOSA A 18, 338–351.
Ciuffi, P., Bayer, B., Berti, M., Franceschini, S., Simoni, A., 2021. Deformation detection in cyclic landslides prior to their reactivation using two-pass satellite interferometry. Appl. Sci. 11, 3156. https://doi.org/10.3390/app11073156.
Cohen-Waeber, J., Bürgmann, R., Chaussard, E., Giannico, C., Ferretti, A., 2018. Spatiotemporal patterns of precipitation-modulated landslide deformation from independent component analysis of InSAR time series. Geophys. Res. Lett. 45 (4), 1878–1887. https://doi.org/10.1002/2017GL075950.
Corsini, A., Farina, P., Antonello, G., Barbieri, M., Casagli, N., Coren, F., Guerri, L., Ronchetti, F., Sterzai, P., Tarchi, D., 2006. Space-borne and ground-based SAR interferometry as tools for landslide hazard management in civil protection. Int. J. Remote Sens. 27 (12), 2351–2369.
Cruden, D.M., Varnes, D.J., 1996. Landslides: investigation and mitigation. Chapter 3-landslide types and processes. In: Transportation Research Board Special Report.
Dini, B., Manconi, A., Loew, S., 2019. Investigation of slope instabilities in NW Bhutan as derived from systematic DInSAR analyses. Eng. Geol. 259, 105111.
Dong, J., Zhang, L., Li, M., Yu, Y., Liao, M., Gong, J., Luo, H., 2018. Measuring precursory movements of the recent Xinmo landslide in Mao County, China with Sentinel-1 and ALOS-2 PALSAR-2 datasets. Landslides 15, 135–144. https://doi.org/10.1007/s10346-017-0914-8.
Fattahi, H., Amelung, F., 2015. InSAR bias and uncertainty due to the systematic and stochastic tropospheric delay. J. Geophys. Res. Solid Earth 120, 8758–8773.
Ferretti, A., Prati, C., Rocca, F., 2001. Permanent scatterers insar interferometry. IEEE Trans. Geosci. Remote Sens. 2001 (39), 8–20.
Ferretti, A., Fumagalli, A., Novali, F., Prati, C., Rocca, F., Rucci, A., 2011. A new algorithm for processing interferometric data-stacks: Squeesar. IEEE Trans. Geosci. Remote Sens. 2011 (49), 3460–3470.
Filippazzo, G., Dinand, S., 2017. The potential impact of small satellite radar constellations on traditional space systems. In: Proceedings of the 5th Federated and Fractionated Satellite Systems Workshop, Ithaca, NY, USA, 2–3 November 2017, p. 12.
Fruneau, B., Achache, J., Delacourt, C., 1996. Observation and modelling of the Saint Etienne-de-tinée landslide using SAR interferometry. Tectonophysics 265, 181–190.
Guzzetti, F., Gariano, S.L., Peruccacci, S., Brunetti, M.T., Marchesini, I., Rossi, M., Melillo, M., 2020. Geographical landslide early warning systems. Earth Sci. Rev. 200, 102973 https://doi.org/10.1016/j.earscirev.2019.102973.
Handwerger, A.L., Roering, J.J., Schmidt, D.A., 2013. Controls on the seasonal deformation of slow-moving landslides. Earth Planet. Sci. Lett. 377, 239–247.
Handwerger, A.L., Roering, J.J., Schmidt, D.A., Rempel, A.W., 2015. Kinematics of earthflows in the northern California coast ranges using satellite interferometry. Geomorphology 246, 321–333.
Handwerger, A.L., Huang, M.-H., Fielding, E.J., Booth, A.M., Bürgmann, R., 2019. A shift from drought to extreme rainfall drives a stable landslide to catastrophic failure. Sci. Rep. 9, 1569.
Hooper, A., 2008. A multi-temporal InSAR method incorporating both persistent scatterer and small baseline approaches. Geophys. Res. Lett. 35, L16302.
Hooper, A., Zebker, H., Segall, P., Kampes, B., 2004. A new method for measuring deformation on volcanoes and other natural terrains using InSAR persistent scatterers. Geophys. Res. Lett. 31.
Hooper, A., Segall, P., Zebker, H., 2007. Persistent scatterer interferometric synthetic aperture radar for crustal deformation analysis, with application to volcán alcedo, galápagos. J. Geophys. Res. Solid Earth 112.
Leroueil, S., Locat, J., Vaunat, J., Picarelli, L., Lee, H., Faure, R., 1996. Geotechnical characterization of slope movements. In: Senneset, K. (Ed.), Landslides, Proceedings 7th International Symposium Landslides, Trondheim, Norway, 17–21 June, 1. Balkema, Rotterdam, The Netherlands, pp. 53–74.
Liu, J.G., Mason, P.J., 2017. Image Processing and GIS for Remote Sensing. Wiley Blackwell, Oxford, UK (457 pp. ISBN: 9781118724200).
Manconi, A., 2021. How phase aliasing limits systematic space-borne DInSAR monitoring and failure forecast of alpine landslides. Eng. Geol. 287, 1–7 (106094).
Massonnet, D., Feigl, K.L., 1998. Radar interferometry and its application to changes in the Earth's surface. Rev. Geophys. 36, 441–500.
Meyer, N.K., Schwanghart, W., Korup, O., Romstad, B., Etzelmüller, B., 2014. Estimating the topographic predictability of debris flows. Geomorphology 207, 114–125. https://doi.org/10.1016/j.geomorph.2013.10.030.
Panini, F., Bettelli, G., Bonazzi, U., Gasperi, G., Fioroni, F., Fregni, P., 2002. Note illustrative alla Carta Geologica d'Italia a scala 1:50.000. Foglio N. 237, Sasso Marconi.
Pavan, V., Tomozeiu, R., Cacciamani, C., Di Lorenzo, M., 2008. Daily precipitation observations over Emilia-Romagna: mean values and extremes. Int. J. Climatol. 28 (15), 2065–2079.
Pini, G.A., 1999. Tectonosomes and olistostromes in the argille scagliose of the Northern Apennines, Italy. Spec. Pap. Geol. Soc. Am. 335 (1), 1–70.
R.E.R., Servizio Geologico, Sismico e dei Suoli, 2022. Landslide Inventory Map 1:10000 scale of the Emilia-Romagna Region, Italy (regularly updated). https://geo.regione.emilia-romagna.it/cartografia_sgss/.
R.E.R., Servizio Statistica e Sistemi Informativi Geografici, 2020. Land use database of the Emilia-Romagna Region, Italy. https://servizimoka.regione.emilia-romagna.it/mokaApp/apps/UDSD/index.html.
Raspini, F., Bianchini, S., Ciampalini, A., Del Soldato, M., Montalti, R., Solari, L., Tofani, V., Casagli, N., 2019. Persistent scatterers continuous streaming for landslide monitoring and mapping: the case of the Tuscany region (Italy). Landslides 16, 2033–2044. https://doi.org/10.1007/s10346-019-01249-w.
Regmi, N.R., Giardino, J.R., Vitek, J.D., 2010. Modeling susceptibility to landslides using the weight of evidence approach: Western Colorado, USA. Geomorphology 115 (1–2), 172–187. https://doi.org/10.1016/j.geomorph.2009.10.002.
Ricci Lucchi, F., 1986. The Oligocene to recent foreland basins of the Northern Apennines. In: A., P., Homewood, P. (Eds.), Special Publication of the International Association of Sedimentologists, vol. 8. Blackwell, Oxford, pp. 105–139.
Ronchetti, F., Borgatti, L., Cervi, F., Lucente, C.C., Veneziano, M., Corsini, A., 2007. The Valoria landslide reactivation in 2005–2006 (Northern Apennines, Italy). Landslides 4 (2), 189–195.
Rosen, P.A., Hensley, S., Joughin, I.R., Li, F.K., Madsen, S.N., Rodriguez, E., Goldstein, R. M., 2000. Synthetic aperture radar interferometry. Proc. IEEE 88, 333–382.
Sandwell, D., Mellors, R., Tong, X., Wei, M., Wessel, P., 2011. Open radar interferometry software for mapping surface deformation. EOS Trans. Am. Geophys. Union 92, 234.
Schmidt, D.A., Bürgmann, R., 2003. Time-dependent land uplift and subsidence in the Santa Clara Valley, California, from a large interferometric synthetic aperture radar data set. J. Geophys. Res. Solid Earth 108.
Simoni, A., Ponza, A., Picotti, V., Berti, M., Dinelli, E., 2013. Earthflow sediment production and holocene sediment record in a large Apennine catchment. Geomorphology 188 (1), 42–53.
Spiegelhalter, D.J., 1986. A statistical view of uncertainty in expert systems. In: Gale, W. (Ed.), Artificial Intelligence and Statistics. Addison-Wesley, Reading, MA, pp. 17–55.
Squarzoni, G., Benedikt, B., Franceschini, S., Simoni, A., 2020. Pre- and post-failure dynamics of landslides in the Northern Apennines revealed by space-borne synthetic aperture radar interferometry (InSAR). Geomorphology 369, 107353.
Tarayre, H., Massonnet, D., 1996. Atmospheric propagation heterogeneities revealed by ERS-1 interferometry. Geophys. Res. Lett. 23, 989–992.
Tomozeiu, R., Busuioc, A., Marletto, V., Zinoni, F., Cacciamani, C., 2000. Detection of changes in the summer precipitation time series of the region Emilia-Romagna, Italy. Theor. Appl. Climatol. 67 (3–4), 193–200.
Tong, X., Schmidt, D., 2016. Active movement of the Cascade landslide complex in Washington from a coherence-based InSAR time series method. Remote Sens. Environ. 186, 405–415.
Torres, R., Snoeij, P., Geudtner, D., Bibby, D., Davidson, M., Attema, E., Potin, P., Rommen, B., Floury, N., Brown, M., Traver, I.N., Deghaye, P., Duesmann, B., Rosich, B., Miranda, N., Bruno, C., L'Abbate, M., Croci, R., Pietropaolo, A., Huchler, M., Rostan, F., 2012. GMES Sentinel-1 mission. Remote Sens. Environ. 120, 9–24. https://doi.org/10.1016/j.rse.2011.05.028.
Trigila, A., Iadanza, C., Spizzichino, D., 2010. Quality assessment of the Italian Landslide Inventory using GIS processing. Landslides 7, 455–470. https://doi.org/10.1007/s10346-010-0213-0.
Vannucchi, P., Maltman, A., Bettelli, G., Clennell, B., 2003. On the nature of scaly fabric and scaly clay. J. Struct. Geol. 25 (5), 673–688.
Xiao, R., Yu, C., Li, Z., Jiang, M., He, X., 2022. InSAR stacking with atmospheric correction for rapid geohazard detection: applications to ground subsidence and landslides in China. Int. J. Appl. Earth Obs. Geoinf. 115, 103082.

Zebker, H.A., Villasenor, J., 1992. Decorrelation in interferometric radar echoes. IEEE Trans. Geosci. Remote Sens. 30, 950–959.
Zebker, H.A., Rosen, P.A., Hensley, S., 1997. Atmospheric effects in interferometric synthetic aperture radar surface deformation and topographic maps. J. Geophys. Res. Solid Earth 102, 7547–7563.
Zhang, Y., Meng, X.M., Dijkstrac, T.A., Jordan, C.G., Chen, G., Zeng, R.Q., Novellino, A., 2020. Forecasting the magnitude of potential landslides based on InSAR techniques. Remote Sens. Environ. 241, 111738.